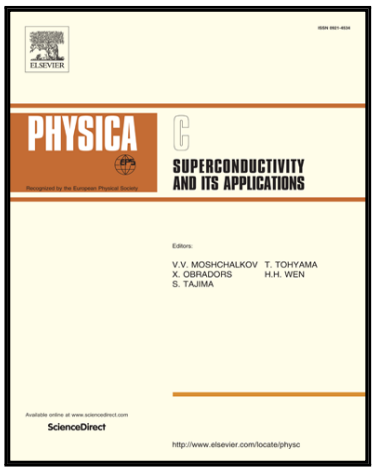

The nematicity induced d-symmetry charge density wave in electron-doped iron-pnictide superconductors

Chung-Pin Chou , Hong-Yi Chen , C.S. Ting

PII: S0921-4534(17)30200-9
DOI: 10.1016/j.physc.2017.12.009
Reference: PHYSC 1253236

To appear in: *Physica C: Superconductivity and its applications*

Received date: 22 September 2017
Revised date: 19 December 2017
Accepted date: 21 December 2017

Please cite this article as: Chung-Pin Chou , Hong-Yi Chen , C.S. Ting , The nematicity induced d-symmetry charge density wave in electron-doped iron-pnictide superconductors, *Physica C: Superconductivity and its applications* (2017), doi: 10.1016/j.physc.2017.12.009

Highlights

- In our study, the nematic state is caused by the anisotropic SDW within FeAs-plane and the topology of Fermi surface. Within this model, we also calculate the phase diagram. In particular, there is a region where the nematic order and superconductivity coexist. This results are able to explain the phenomena that the spin anisotropy is enhanced upon entering into the superconducting state.
- In our calculation, we choose the different configurations of the staggered magnetization M_i to study the states driven by the magnetic mechanism. The magnetic configuration is described as,
    - $M_i = M_1 \cos(q_y \cdot r_i)\, e^{iQ_x \cdot r_i} + M_2 \sin(q_x \cdot R)\, e^{iQ_y \cdot r_i}$.

  In the stripe SDW state, the ordering vector is chosen as either Q_x or Q_y, which is consistent with Fernandez's model. However, in the nematic state, we use both order vectors Q_x and Q_y, and extra wave vectors q_x and q_y, instead of single-Q value in Fernandez's model. Accordingly, the nematic state could be attributed to two inequivalent stripes with the same period of the modulation interpenetrating each other. This configuration includes two Q and q values. The two Q values are responsible for two stripes with 90° rotation difference and the two q values result in the modulation on each stripe. The advantage by choosing Q and q vectors is that one can have a stabilized magnetic configuration in real space. The corresponding momentum space of the spin configurations also exhibit the properties of the nematic order, such as $\langle \Delta_x \rangle = \langle \Delta_y \rangle = 0$ and $\langle \Delta_x^2 \rangle \neq \langle \Delta_y^2 \rangle$. Therefore, one can easily use the spatial configuration to study several properties such as the spectroscopic imaging (LDOS map).
- To compare with the STM experiements, we have two results in our calculations. One is the $d\mathrm{I}/d\mathrm{V}$ spectrum and the other is the spectroscopic imaging (the LDOS map). In cuprate, the *atomic-scale* electronic structure has shown a d-wave like symmetry (PNAS 111,E3026 (2014), Nat. Phys. 12, 150 (2016)). The Fourier transforms also show four peaks around the center of the momentum space. Such an *atomic-scale* feature in cuprates has not yet been reported in iron-pnictides. Besides, the report of the $d\mathrm{I}/d\mathrm{V}$ spectrum still lacks in the nematic state.

The nematicity induced *d*-symmetry charge density wave in electron-doped iron-pnictide superconductors

Chung-Pin Chou[1], Hong-Yi Chen*[1,2] and C. S. Ting[2]

[1]*Department of Physics, National Taiwan Normal University, Taipei, 116, Taiwan*

[2]*Department of Physics and Texas Center for Superconductivity, University of Houston, Houston, Texas 77204, USA*

Email: hongyi@ntnu.edu.tw

(Revised 21 December 2017)

The interplay among the nematicity, the stripe spin-density-wave (SDW) order and superconductivity in iron-pnictides is studied in a self-consistent Bogoliubov-de Gennes equations. Our calculations have shown that the nematic-order breaks the degeneracy of d_{xz} and d_{yz} orbitals and causes the elliptic Fermi surface near the Γ point in the normal state. In addition, the appearance of the orthorhombic magnetic fluctuations generates two uneven pairs of peaks at $(\pm\pi, 0)$ and $(0, \pm\pi)$ in its Fourier transformation. All these are comparing favorably with experimental measurements. In the nematic phase, our results indicate that the charge density and its spatial image in the local density of states exhibit a $d_{x^2-y^2}$-like symmetry. Finally, the complete phase diagram is obtained and the nematic phase is found to be in a narrow region close to the SDW transition in the electron-doped iron-pnictide superconductors.

PACS numbers: 74.70.Xa, 74.20.Mn, 74.25.Jb

I. INTRODUCTION

In common with copper-like superconductors, the emergency of superconductivity in electron-doped Fe-pnictides such as $\mathrm{Ba(Fe_{1-x}Co_xAs)_2}$ is to suppress the magnetic order and fluctuations originated in the parent compound with $x = 0$. In both pnictides and cuprates, the experimentally observed nematicity exists in an exotic phase between the superconductivity (SC) and the stripe spin density wave (SDW) [1]. The relation between SC and the nematicity has become one of the essential issues in the Fe-based superconductors.

The nematic phase is characterized by an underlying electronic order that spontaneously breaks tetragonal symmetry [2-16]. In iron-pnictides, the nematic order has been proposed to arise from the spin fluctuations [17-21] or charge fluctuations [22,23]. The spin driven nematicity picture has been proven by the spin-polarized inelastic neutron scattering (SP-INS) experiments [24,25]. The properties of the spin-driven nematic order in the normal state have been widely studied. However, recently, the SP-INS experiments have pointed out that the optimally doped samples [26,27] in the superconducting state shows the similar behavior of the resonance peaks to the gap modes of the parent compounds [28] in the stripe SDW state. In addition, the SP-INS experiments also revealed the enhanced in-plane spin anisotropy upon entering into the superconducting state [29]. Although the normal state has attracted a lot of attentions, the microscopic description of the nematic order and particularly, the relation between SC and the nematic order are still missing. It is also worth mentioning that the longitudinal spin excitations are identified implying that the spin anisotropy is caused by the contribution of itinerant electrons and the topology of Fermi surface.

In the itinerant picture, the magnetic configuration in FeSCs can be described in terms of two magnetic order parameters Δ_x and Δ_y. The order parameters defined in momentum space are written as [30],

$$\Delta_\ell = \sum_k c^\dagger_{k+Q_\ell,\alpha}\sigma_{\alpha\beta}c_{k,\beta}$$

where $\ell = x$ or y. Here $Q_x = (\pi, 0)$ corresponds to the spins parallel along the y-axis and antiparallel along the x-axis. and $Q_y = (0, \pi)$ corresponds to the spins parallel along the x-axis and antiparallel along the y-axis. $\langle\Delta_\ell\rangle \neq 0$ corresponds to the breaking of the $O(3)$ spin rotational symmetry and $\langle\Delta_x^2\rangle \neq \langle\Delta_y^2\rangle$ corresponds to the C_4 lattice rotational symmetry broken. In the stripe SDW state, the magnetic ground state is an orthorhombic uniaxial stripe state, i.e. $\langle\Delta_x\rangle \neq 0$ or $\langle\Delta_y\rangle \neq 0$. This order breaks the $O(3)$ symmetry. In real space, the stripe order reduces the point-group symmetry of a unit cell from C_4 (tetragonal) to C_2 (orthorhombic) by choosing the ordering vector either Q_x or Q_y. In the nematic state, the $O(3)$ symmetry is preserved and the C_4 (tetragonal) symmetry is broken. The order parameters have $\langle\Delta_x\rangle = \langle\Delta_y\rangle = 0$ and the fluctuations associated with one of the ordering vectors are stronger than the other $\langle\Delta_x^2\rangle > \langle\Delta_y^2\rangle$ or $\langle\Delta_y^2\rangle > \langle\Delta_x^2\rangle$. In real space, the x and y directions are inequivalent. The magnetic fluctuations induce the tetragonal symmetry-breaking and trigger the transition from a tetragonal to an orthorhombic phase.

On the one hand, the structural orders driven by magnetic fluctuations are usually referred to Ising-nematic phase where the Z_2 symmetry is broken but the $O(3)$ spin-rotational symmetry is not [20]. The Z_2 symmetry indicates to the degenerate of the spin stripes along the y-axis (corresponding to Q_x) or x-axis (corresponding to Q_y). The breaking Z_2 symmetry by choosing either Q_x or Q_y implies a tetragonal-to-orthorhombic transition. On the other hand, recently, the reentrant C_4 symmetry magnetic order found in hole doped Fe-pnictide [31-33] has been explained in the double-Q order (choose both Q_x and Q_y). The double-Q order is proposed to change the ground state from stripe to tetragonal [34,35]. In real space, the double-Q order simply indicates the superposition of two

stripe SDW order with the ordering vectors Q_x and Q_y. However, such a superposition would end up to an order with (π,π) and preserve the tetragonal symmetry. An additional modulation, nevertheless, is needed in the double-Q order to break the lattice rotational symmetry.

In this paper, we study the interplay between SC and nematicity by a two-orbital Hamiltonian with the double-Q order in a two-dimensional lattice. Two orbitals d_{xz} and d_{yz} equally contribute to the spin fluctuations in the stripe SDW phase, whereas the unequal contributions between both orbitals break the C_4 point-group symmetry in the nematic phase. The mechanism behind the fluctuations of d_{xz} and d_{yz} orbitals can be understood from an extended RPA approach where d_{xz}, d_{yz}, and d_{xy} orbitals equally contribute to the SDW instability, and in particular the d_{xy} orbital play a strong role in the nematic instability [17]. For the sake of convenience of calculations, a two-orbital model has been successful in many applications incorporate the SC, such as quasiparticle excitation, the density of states near an impurity and the magnetic structure of a vortex core [36].

The rest of paper is organized as follows. In Sec. II, we use a two-orbital Hamiltonian in a square lattice and apply the mean-field scheme. The nematic order is proposed in the magnetic configuration. The phase diagram, band structure, and the Fermi surface are calculated. In Sec. III, we numerically solve the Bogoliubov-de Gennes (BdG) equations and then calculate the local density of states. In Sec. IV, we present a summary of the results.

II. MODEL

The multi-orbital Hamiltonian of the iron-pnictide superconductors in a two-dimensional square lattice is described as,

$$H=\sum_{ijuv\alpha}t_{ijuv}c_{iu\alpha}^{\dagger}c_{jv\alpha}-\mu\sum_{iu\alpha}n_{iu\alpha}+U\sum_{iu}n_{iu\uparrow}n_{iu\downarrow}+\left(U'-J_H/2\right)\sum_{iu<v\alpha\beta}n_{iu\alpha}n_{iv\beta}-2J_H\sum_{iu<v}S_{iu}\cdot S_{iv}+J'\sum_{iu\neq v}c_{iu\uparrow}^{\dagger}c_{iu\downarrow}^{\dagger}c_{iv\downarrow}c_{iv\uparrow},$$

where the operators $c_{iu\alpha}^{\dagger}$ ($c_{iu\alpha}$) create (annihilate) an ectron with spin $\alpha,\beta=\uparrow,\downarrow$ in the orbital $u,v=1,2$ on the lattice site i; t_{ijuv} is the hopping matrix elements between the neighbor sites and μ is the chemical potential. $n_{iu\alpha}=c_{iu\alpha}^{\dagger}c_{iu\alpha}$ and $S_{iu}=\frac{1}{2}\sum_{\alpha\beta}c_{iu\alpha}^{\dagger}\sigma_{\alpha\beta}c_{iu\beta}$ with $\sigma_{\alpha\beta}$ the Pauli matrices. U (U') is the intraorbital (interorbital) on-site interaction. The Hund's rule coupling is J_H and the pair hopping energy is J'. The spin-rotation invariance gives $U'=U-2J_H$ and $J'=J_H$ [37]. Repulsion between electrons requires $J_H<U/3$.

In a two-orbital model, the hopping amplitudes are chosen as $t_{1-6}=(-1,0.08,1.35,-0.12,0.09,0.25)$ [38] to fit the band structure from the first-principles calculations.

$$t_1=t_{i,i\pm x(y),u,u}=-1,$$

$$\begin{cases}t_{i,i\pm(x+y),u,u}=\dfrac{1+(-1)^{x+y+u}}{2}t_2+\dfrac{1-(-1)^{x+y+u}}{2}t_3=0.08,\\ t_{i,i\pm(x-y),u,u}=\dfrac{1+(-1)^{x-y+u}}{2}t_3+\dfrac{1-(-1)^{x-y+u}}{2}t_2=1.35,\end{cases}$$

$$t_4=t_{i,i\pm(x\pm y),u,v\neq u}=-0.12,$$

$$t_5 = t_{i,i\pm x(y),u,v\neq u} = 0.09,$$
$$t_6 = t_{i,i\pm 2x(2y),u,u} = 0.25,$$

where $u \neq v$. On the same orbital, t_2 and t_3 are chosen differently along the mutually perpendicular directions. t_2 and t_3 are twisted between sublattices. The C_4 symmetry on the same orbital between different sublattices is broken. Furthermore, on the same sublattice, t_2 and t_3 are twisted again and the degeneracy between d_{xz} and d_{yz} orbitals is broken. The combined effects of conditions of t_2 and t_3 on the same orbitals and sublattices restore the C_4 symmetry of the lattice structure. Figure 1(a) and 1(b) display the Fermi surface and the band structure in the absence of SDW. The Fermi surface contains two hole pockets around the Γ point and two electron pockets around the M points. The Fermi surface exhibits the C_4 symmetry of the lattice structure. The nature of these Fermi surface pockets is revealed by the line at the Fermi energy crossing the band dispersion around Γ and M points.

In the mean-field level,

$$H = H_0 + H_\Delta + H_{\text{int}}$$

the Hamiltonian is self-consistently solved accompanied with s^{+-}-wave superconducting order. The mean-field scheme is the same as Ref. [38].

$$H_0 = \sum_{ijuv\alpha} t_{ijuv} c^\dagger_{iu\alpha} c_{jv\alpha} - \mu \sum_{iu\alpha} n_{iu\alpha}$$

$$H_\Delta = \sum_{iju\alpha} \left(\Delta_{iju} c^\dagger_{iu\alpha} c_{ju\beta} + \text{h.c.} \right)$$

$$H_{\text{int}} = U \sum_{iu,\alpha\neq\beta} \langle n_{iu\beta} \rangle n_{iu\alpha} + U' \sum_{i,u<v,\alpha\neq\beta} \langle n_{iu\beta} \rangle n_{iv\alpha} + \left(U' - J_H \right) \sum_{iu<v,\alpha} \langle n_{iu\alpha} \rangle n_{iv\alpha}$$

The superconducting order parameter $\Delta_{iuu} = V\langle c_{i\uparrow} c_{j\downarrow} \rangle$ results from the next nearest-neighbor intra-orbital attractive interactions V [39-41]. We choose the parameters of interactions $U = 3.5$, $J_H = 0.4$, and $V = 1.3$. It is found that $U \geq 3.5$ is able to induce the nematic order within a small doping range near the maximum superconducting order, instead of a uniform SDW order [38,41] where U is chosen to be 3.2.

In a lattice, we choose the different configurations of the staggered magnetization M_i to study the states driven by the magnetic mechanism. The magnetic configuration is described as,

$$M_i = M_1 \cos(q_y \cdot r_i)\, e^{iQ_x \cdot r_i} + M_2 \sin(q_x \cdot R)\, e^{iQ_y \cdot r_i}$$

where the wavevectors $q_x = (2\pi/\lambda, 0)$ and $q_y = (0, 2\pi/\lambda)$ correspond to a modulation along the *x*-axis and the *y*-axis with wavelength λ. M_1 and M_2 are the amplitude of the modulation. In the stripe SDW state, $M_1 = 0$ or $M_2 = 0$ are chosen to break the C_4 symmetry, which is equivalent to choose the ordering vector either Q_x or Q_y, consistent with the single-Q model [14,18,21]. In the nematic state, the preserving of the C_2 symmetry makes the *x*- and *y*-directions inequivalent, i.e. $M_1 \neq M_2$. The modulated antiparallel spins along the *x*-axis and the *y*-axis imply

$\langle\Delta_x\rangle = \langle\Delta_y\rangle = 0$ and $\langle\Delta_x^2\rangle \neq \langle\Delta_y^2\rangle$. Within the periodic boundary conditions, the value of q must commensurate the lattice to stabilize the modulation and lower the energy of the system. Accordingly, the nematic state could be attributed to two inequivalent stripes with the same period of the modulation interpenetrating each other. This configuration including two Q and q values extends the double-Q model [34]. The two Q values are responsible for two stripes with 90° rotation difference and the two q values result in the modulation on each stripe. As the modulations along the *x*- and *y*- directions have no phase difference, the configuration of the SDW implies a *s*-symmetric form factor. On the other hand, as the modulations have a phase shift of $\pi/2$, the spin configuration implies a *d*-symmetric form factor.

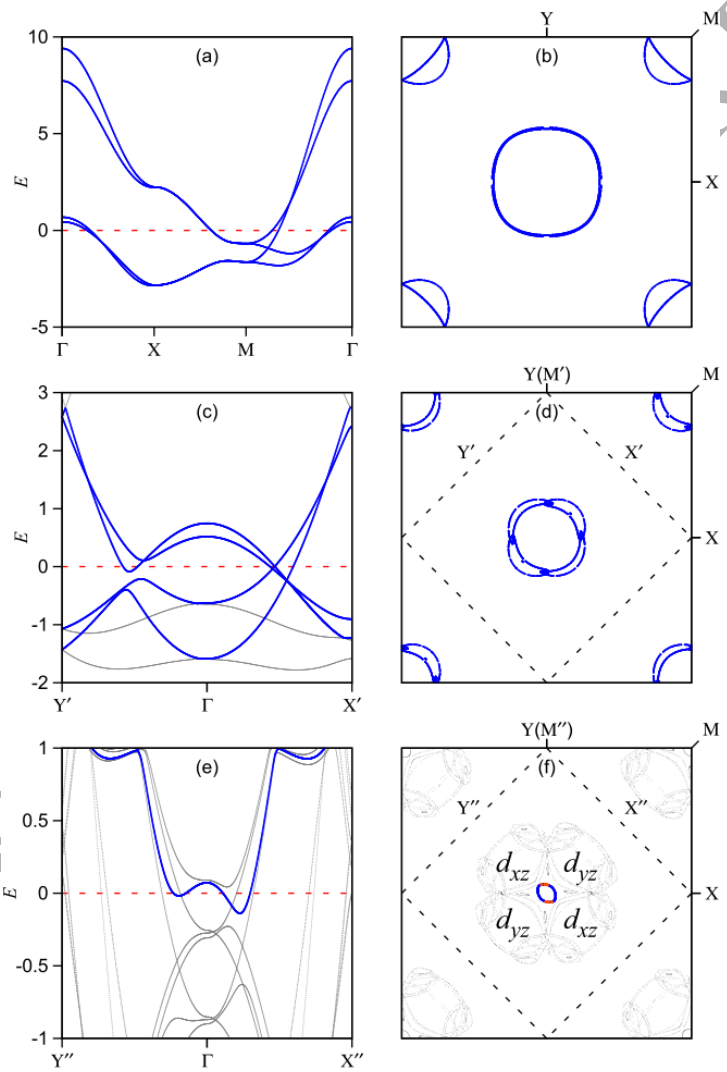

FIG. 1. (Color online) (a) and (b) are, respectively, the band structure and the Fermi surface without SDW. The Fermi energy (red dashed line) corresponds to the electron filling $n = 2.1$. (c) and (d) are, respectively, the band structure and the Fermi surface in the stripe SDW state. The Fermi energy (red dashed line) corresponds to the electron filling $n = 2.04$. (e) and (f) are, respectively, the band structure and the Fermi surface in the nematic state. The asymmetric band (blue color) is responsible for the elliptic Fermi surface around the Γ point. The blue and red

solid curves represent the major contributions from the orbitals d_{xz} and d_{yz}, respectively. The chemical potential is chosen as the electron filling $n = 2.1$. The black dashed lines in (d) and (f) represent the magnetic Brillouin zone. X′ and X″ indicate the x-direction in the magnetic Brillouin zone.

Figure 1 displays the band structure and the Fermi surface of the state without SDW, the stripe SDW state, and the nematic state. In the study of the Fermi surface, the superconductivity is set to zero because the superconductivity mainly opens a gap on parts of the Fermi surface where there is no SDW gap. In the absence of SDW, the hole bands are centered at Γ point and the electron bands are centered at M point. There is no gap in the band structure. The Fermi surface has C_4 symmetry at filling $n = 2.1$ (as shown in Fig. 1(a) and 1(b)). In the stripe SDW state, the SDW has an intimate impact on the surface topology. Fig. 1(c) shows a gap along the Y′-direction and gapless along the X′-direction. This indicates that the magnetic configuration has antiparallel spins (antiferromagnetism) along the X′-direction and parallel spins (ferromagnetism) along the Y′-direction [25]. The Fermi surface at filling $n = 2.04$ is displayed in Fig. 1(d). There are four hole-pockets around the Γ point. The pockets along the $\Gamma - Y'$ direction is inequivalent to the one along the $\Gamma - X'$ direction.

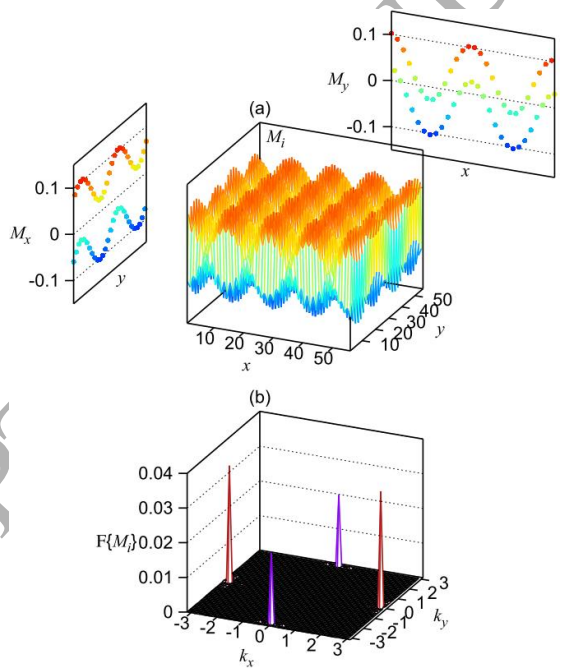

FIG. 2. (Color online) (a) The real space configurations of the magnetization M_i are plotted on a 56×56 square lattice. The left and the right panels are the sliced profile along the peaks along the *y*- and *x*-directions, respectively. Two curves show in both panels. The upper and lower curves represent the spin-up and spin-down configurations, respectively. (b) The Fourier transformation of the spatial magnetic configuration.

In the nematic state, the antiparallel spins along both the X″ and Y″ directions. There is no gap in the band structure. In particular, there is one band exhibiting the asymmetry (blue color) with respect to the Γ point. The asymmetric band shape results from the inequivalent value of M_1 and M_2. As $M_1 > M_2$, the band along the Y″

direction is lifted higher (blue curve in figure 1(e)). The Fermi surface is depicted at filling $n = 2.1$. The elliptic hole-pocket in the Fermi surface near the Γ point is due to the asymmetry band. Furthermore, the nematicity breaks the degeneracy of two iron-orbitals d_{xz} and d_{yz}. Orbitals d_{xz} and d_{yz} have the uneven contributions to the charge distributions $n_{xz}(k)$ and $n_{yz}(k)$ (blue and red curves in Fig. 1(f)). The fluctuations of orbitals d_{xz} and d_{yz} are induced from the nematic fluctuations. These results are able to explain the anisotropic Fermi surface reported by the angular-resolved-photoemission-spectroscopy (ARPES) experiments [3].

III. NEMATICITY IN REAL SPACE

We, further, self-consistently solve the BdG equations for different SDW states in two-dimensional square lattice:

$$\sum_{jv}\begin{pmatrix} H_{ijuv\uparrow} & \Delta_{ijvv} \\ \Delta^{*}_{ijvv} & H^{*}_{ijuv\downarrow} \end{pmatrix}\begin{pmatrix} u^{n}_{jv\uparrow} \\ v^{n}_{jv\downarrow} \end{pmatrix} = E_{n\uparrow}\begin{pmatrix} u^{n}_{iu\uparrow} \\ v^{n}_{iu\downarrow} \end{pmatrix},$$

where

$$H_{iju\alpha} = t_{iju\alpha} + \{-\mu + U\langle n_{iu\beta}\rangle + U'\langle n_{iv\alpha}\rangle + (U' - J_H)\langle n_{iv\beta}\rangle\}\delta_{ij}$$

and $U' = U - 2J_H$. The self-consistency conditions are

$$\langle n_{iu\uparrow}\rangle = \sum_{n} |u^{n}_{iu\uparrow}|^2 f(E_n)$$

$$\langle n_{iu\downarrow}\rangle = \sum_{n} |v^{n}_{iu\downarrow}|^2 f(1 - E_n)$$

$$\Delta_{ijuu} = \frac{V}{2}\sum_{n} u^{n}_{iu\uparrow} v^{n*}_{iu\downarrow} \tanh\left(\frac{\beta E_n}{2}\right)$$

Here, $f(E_n)$ is the Fermi distribution function.

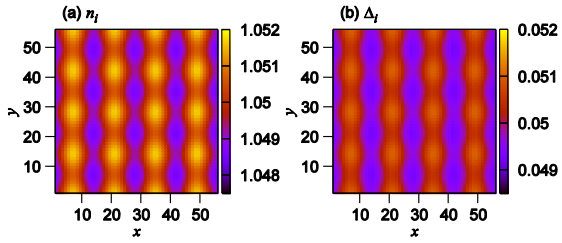

FIG. 3. (Color online) (a) The spatial configuration of the electronic charge density n_i. (b) The spatial configuration of the s^{+-}-wave superconducting order parameter Δ_i.

Figure 2(a) displays the spatial fluctuations of the magnetization M_i in coexisting state of the nematic order and SC. The slided profile along the peaks along the *x*- or *y*-direction reveals a sinusoidal modulation. The left panel

illustrates the modulated staggered magnetization $M_1 \cos(q_y \cdot r_i)$ with $M_1 \cong 0.04$. The right panel illustrates the modulated staggered magnetization $M_2 \sin(q_x \cdot r_i)$ with $M_2 \cong 0.06$. The corresponding wavelength of the modulation is $\lambda_x = \lambda_y = 28a$ along both the *x*- and *y*-directions. These results indicate an orthorhombic spin configuration, i.e. the broken of the 90° rotational symmetry.

The Fourier transformation of the spatial configuration of the nematic fluctuations is shown in Figure 2(b). There are four peaks exhibiting at $(\pm\pi, 0)$ and $(0, \pm\pi)$. The two pairs of peaks have inequivalent intensities. The intensities of one pair of peaks at $(\pm\pi, 0)$ (ordering vector Q_x) is larger than the other pair at $(0, \pm\pi)$ (ordering vector Q_y). The nonequivalence of the intensities between the x- and y-pairs indicates $\langle\Delta_x\rangle = \langle\Delta_y\rangle = 0$ and $\langle\Delta_y^2\rangle > \langle\Delta_x^2\rangle$ [19]. The features in momentum space indicates that the modulated antiparallel spin configuration is able to represent the nematic state. Our numerical calculation also indicates that the features exhibited in Figure 2(b) would not be affected by the absence of the SC phase. This result is in agreement with the neutron scattering experiments [2,9], and so far this is the only work that is able to microscopically explain these experiments.

In the nematic state, $\langle\Delta_y^2\rangle > \langle\Delta_x^2\rangle$ in momentum space indicates that two inequivalent modulated stripes along the *x*- and *y*-direction orthogonally intertwined with each other (see Figure 2). A correspondingly two-fold symmetric checkerboard-like pattern appears in real space. In Figures 3(a) and 3(b), our numerically calculated electronic charge density $n_i = (n_{i\uparrow} + n_{i\downarrow})$ and the s^{+-}-wave SC order-parameter Δ_i are displaced in real space respectively. Unlike the stripe SDW state, where there is no charge density wave exhibited, the nematicity of the spin order induces a modulated charge density wave (CDW) with period $14a$ (half period of the magnetization) in x- and y- directions. The CDW consisting of crisscrossed horizontal and vertical stripes forms a check plaid pattern, instead of a checkerboard pattern, i.e. the CDW exhibits a $d_{x^2-y^2}$-symmetry, instead of a d_{xy}-symmetry, form factor density wave. While the amplitudes along the *x* direction and along the *y* direction are nonequivalent, which makes four-fold symmetric check plaid pattern becomes a two-fold symmetric pattern. As shown in Figure 3(a) and 3(b), both the magnetic induced charge density wave n_i and pair density wave Δ_i display the same two-fold *d*-symmetric pattern in the nematic state.

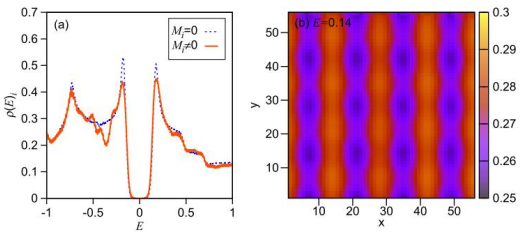

FIG. 4. (Color online) (a) The LDOS in the nematic state. The dashed (blue) line represents the LDOS without magnetization ($M_i = 0$). (b) The LDOS map at $E = 0.14$.

The local density of states (LDOS) proportional to the differential tunneling conductance as measured by STM is expressed as,

$$\rho_i(E) = \frac{-1}{N_x N_y} \sum_{nu} \left[\left| u^n_{iu\uparrow} \right|^2 f'(E_n - E) + \left| v^n_{iu\downarrow} \right|^2 f'(E_n + E) \right]$$

where $N_x \times N_y = 24 \times 24$ are the size of supercells. In the striped SDW state, in the electron-doped regime, the SDW gaps shifts toward negative energy. The intensities of superconducting coherence peaks at the positive and negative energies are respectively unchanged and suppressed. This is a prominent feature caused by the magnetic SDW order that the intensities of superconducting coherence peaks are obvious asymmetry [41]. In the nematic state, the modulation along the antiparallel spins leads to a gapless features in the band structure, i.e. no SDW gap. The only gap appears in the LDOS is the superconducting gap. In addition, the competition between the nematic order and the superconducting order results in the suppression of the superconducting coherence peaks as shown in Figure 4(a). Furthermore, the spatial distribution of LDOS at $E = 0.14$ (spectroscopic-imaging or LDOS map) is presented in Figure 4(b). The LDOS map shows a check plaid pattern with a $d_{x^2-y^2}$-symmetric form factor. In cuprate, the atomic-scale electronic structure has also shown a d-wave like symmetry [43,44]. Such an atomic-scale feature has not yet been reported in iron-pnictides.

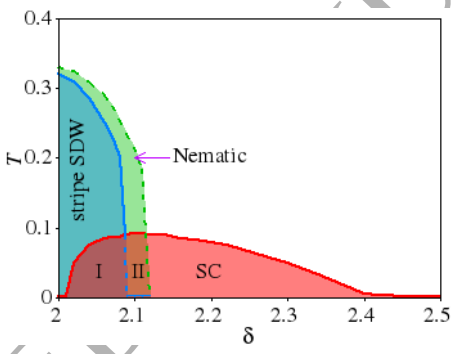

FIG. 5. (Color online) The phase diagram of the stripe SDW order (blue), nematic order (green) and superconducting order (red) as a function of doping.

Figure 5 displays the phase diagram of the stripe SDW order, nematic order and s^{+-}-wave superconducting order as a function of doping obtained from the self-consistent calculation. In our calculation, T is set in unit of $|t_1|$ (the hopping integral). The phase diagram is deduced as follows. For the superconducting dome, the T_c is determined as the site average magnitude of Δ_i approaches to zero. For the zone boundary of the nematic order, since the nematic order is driven by the spin fluctuations, the region between T_s (structural transition temperature) and T_N (Neel temperature) would follow up the doping dependence of stripe SDW state. The upper bound of the nematicity is determined by the nematic order parameter $\phi \propto \langle \Delta_y^2 - \Delta_x^2 \rangle$. As $\phi \simeq 0$, the corresponding spatial magnetic fluctuations have $M_1 = M_2$ indicating T_s. The lower bound or the boundary between the stripe SDW state and the nematic state is determined by comparing the free energy of the stripe SDW state and the nematic state, which indicates T_N.

In the electron-doped region, the SC (red curve) rapidly increases and reaches the maximal value at $n = 2.1$, and then decreases to almost zero around $n = 2.4$. The stripe SDW order (blue curve) diminishes swiftly around $n = 2.08$. The green area represents a nematic phase where the nematic trantition line (dashed curve) tracks closely the stripe SDW transition line. In particular, the areas denoted "I" and "II" representing the stripe SDW and nematic order coexist with the SC, respectively. The phase diagram is in good agreement with the experiments [45]. The ground state of the stripe SDW and its coexisting state (region I), exhibits the magnetic structure with single-Q order (one ordering vector Q_x or Q_y), i.e., $\langle\Delta_x\rangle = 0$ or $\langle\Delta_y\rangle = 0$. Remarkably, the ground state of the coexisting nematic phase (region II), illustrates a spin structure characterized by two ordering vectors Q_x and Q_y and two modulating vectors q_x and q_y with different amplitudes, i.e., $\langle\Delta_x\rangle = \langle\Delta_y\rangle = 0$ and $\langle\Delta_x^2 - \Delta_y^2\rangle \neq 0$.

IV. CONCLUSION

In conclusion, we have studied the interplay among the nematic, SDW, and SC orders in electron-doped iron-pnictide superconductors such as $Ba(Fe_{1-x}Co_xAs)_2$ using a two-orbital tight-binding model plus the magnetic interactions [38]. The complete phase diagram is obtained and the nematic state only exists in a narrow region close to the SDW transition, in agreement with the experiments [41]. In the nematic and the normal state, the broken degeneracy of the orbitals d_{xz} and d_{yz} causes the formation of the elliptic Fermi-surface near the Γ point, and this is consistent with the ARPES experiments [3]. In the nematic state with or without the SC phase, an orthorhombic magnetic fluctuations in real space appears and its Fourier transformation shows two uneven pairs of peaks at $(\pm\pi, 0)$ and $(0, \pm\pi)$ as shown in Figure 3(b). This result so far has not been micrscopically obtained by other mechanisms, and for the first time, we have, the theory that is able to successfully explain the neutron scattering experiments [2, 9]. In the nematic state, we predict that the charge density and its LDOS map become non-uniform, and exhibit a $d_{x^2-y^2}$-like symmetry in their form factor. Hopefully the prediction could be tested by future scanning tunneling experiments.

ACKNOWLEDGEMENTS

The authors would like to thank Y.R. Chen and M.C. Chang for useful discussion and L.H. Pan for partial technical support. H.Y.C. was supported by MoST of Taiwan under Grant No. 104-2112-M-003-003-MY3 and 102-2112-M-002-003-MY3, and National Center for Theoretical Science of Taiwan. C.S.T. was supported by the Texas Center for Superconductivity at the University of Houston and the Robert A. Welch Foundation under the Grant NO. E-1146

[1] J. C. Séamus Davis and Dung-Hai Lee, PNAS 110, 17623 (2013).

[2] J. Zhao, D. T. Adroja, D. X. Yao, R. Bewley, S. L. Li, X. F. Wang, G. Wu, X. H. Chen, J. P. Hu, and P. C. Dai, Nature Phys. 5, 555 (2009).

[3] Ming Yi, Donghui Lu, Jiun-Haw Chu, James G. Analytis, Adam P. Sorini, Alexander F. Kemper, Brian Moritz, Sung-Kwan Mo, Rob G. Moore, Makoto Hashimoto, Wei-Sheng Lee, Zahid Hussain, Thomas P. Devereaux, Ian R. Fisher, and Zhi-Xun Shen, PNAS 108, 6878 (2011).

[4] T.-M. Chuang, M. P. Allan, Jinho Lee, Yang Xie, Ni Ni, S. L. Bud ' ko, G. S. Boebinger, P. C. Canfield, and J. C. Davis, Science 327, 181 (2010).

[5] Jiun-Haw Chu, James G. Analytis, Kristiaan De Greve, Peter L. McMahon, Zahirul Islam, Yoshihisa Yamamoto, and Ian R. Fisher, Science 329, 824 (2010).

[6] Jiun-Haw Chu, James G. Analytis, David Press, Kristiaan De Greve, Thaddeus D. Ladd, Yoshihisa Yamamoto, and Ian R. Fisher, Phys. Rev. B 81, 214502 (2010).

[7] T. Shimojima, K. Ishizaka, Y. Ishida, N. Katayama, K. Ohgushi, T. Kiss, M. Okawa, T. Togashi, X.-Y. Wang, C.-T. Chen, S. Watanabe, R. Kadota, T. Oguchi, A. Chainani, and S. Shin, Phys. Rev. Lett. 104, 057002 (2010).

[8] M. A. Tanatar, E. C. Blomberg, A. Kreyssig, M. G. Kim, N. Ni, A. Thaler, S. L. Bud'ko, P. C. Canfield, A. I. Goldman, I. I. Mazin, and R. Prozorov, Phys. Rev. B 81, 184508 (2010).

[9] L. W. Harriger, H. Q. Luo, M. S. Liu, C. Frost, J. P. Hu, M. R. Norman, and Pengcheng Dai, Phys. Rev. B 84, 054544 (2011).

[10] M. Nakajima, T. Liang, S. Ishida, Y. Tomioka, K. Kihou, C. H. Lee, A. Iyo, H. Eisaki, T. Kakeshita, T. Ito, and S. Uchida, PNAS 108, 12238 (2011).

[11] Hsueh-Hui Kuo, Jiun-Haw Chu, Scott C. Riggs, Leo Yu, Peter L. McMahon, Kristiaan De Greve, Yoshihisa Yamamoto, James G. Analytis, and Ian R. Fisher, Phys. Rev. B 84, 054540 (2011).

[12] S. Kasahara, H. J. Shi, K. Hashimoto, S. Tonegawa, Y. Mizukami, T. Shibauchi, K. Sugimoto, T. Fukuda, T. Terashima, Andriy H. Nevidomskyy, and Y. Matsuda, Nature 486, 382 (2012).

[13] Jiun-Haw Chu, Hsueh-Hui Kuo, James G. Analytis, and Ian R. Fisher, Science 337, 710 (2012).

[14] Rafael M. Fernandes, Anna E. Böhmer, Christoph Meingast, and Jörg Schmalian, Phys. Rev. Lett. 111, 137001 (2013).

[15] E. C. Blomberg, M. A. Tanatar, R. F. Fernandes, I. I. Mazin, B. Shen, H.-H. Wen, M. D. Johannes, J. Schmalian, and R. Prozorov, Nature Comm. 4, 1914 (2013).

[16] C. Mirri, A. Dusza, S. Bastelberger, J.-H. Chu, H.-H. Kuo, I. R. Fisher, and L. Degiorgi, Phys. Rev. B 90, 155125 (2014).

[17] Morten H. Christensen, Jian Kang, Brian M. Andersen, and Rafael M. Fernandes, Phys. Rev. B 93, 085136 (2016).

[18] R. M. Fernandes, A. V. Chubukov and J. Schmalian, Nature Phys. 10, 97 (2014).

[19] R. M. Fernandes, A. V. Chubukov, J. Knolle, I. Eremin, and J. Schmalian, Phys. Rev. B 85, 024534 (2012).

[20] J. P. Hu and C. Xu, Physica C 481, 215 (2012).

[21] R. M. Fernandes and J. Schmalian, Supercond. Sci. Technol. 25, 084005 (2012).

[22] W. Lv and P. Phillips, Phys. Rev. B 84, 174512 (2011).

[23] W.-C. Lee and P. W. Phillips, Phys. Rev. B 86, 245113 (2012).

[24] Xingye Lu, J. T. Park, Rui Zhang, Huiqian Luo, Andriy H. Nevidomskyy, Qimiao Si, Pengcheng Dai, Science 345, 657 (2014).

[25] Wenliang Zhang, J. T. Park, Xingye Lu, Yuan Wei, Xiaoyan Ma, Lijie Hao, Pengcheng Dai, Zi Yang Meng, Yi-feng Yang, Huiqian Luo, and Shiliang Li, Phys. Rev. Lett. 117, 227003 (2016).

[26] N. Qureshi, P. Steffens, S. Wurmehl, S. Aswartham, B. Buchner, and M. Braden, Phys. Rev. B 86, 060410(R) (2012).

[27] Chong Wang, Rui Zhang, Fa Wang, Huiqian Luo, L. P. Regnault, Pengcheng Dai, and Yuan Li, Phys. Rev. X 3 041036 (2013).

[28] P. Steffens, C. H. Lee, N. Qureshi, K. Kihou, A. Iyo, H. Eisaki, and M. Braden, Phys. Rev. Lett. 110, 137001 (2013).

[29] Huiqian Luo, Meng Wang, Chenglin Zhang, Xingye Lu, Louis-Pierre Regnault, Rui Zhang, Shiliang Li, Jiangping Hu, and Pengcheng Dai, Phys. Rev. Lett.111, 107006 (2013).

[30] A. B. Vorontsov, M. G. Vavilov, and A. V. Chubukov, Phys. Rev. B 79, 060508(R) (2009).

[31] S. Avci, O. Chmaissem, J. M. Allred, S. Rosenkranz, I. Eremin, A.V. Chubukov, D. E. Bugaris, D. Y. Chung, M. G. Kanatzidis, J.-P Castellan, J. A. Schlueter, H. Claus, D. D. Khalyavin, P. Manuel, A. Daoud-Aladine, R. Osborn, Nature Comm. 5, 3845 (2014).

[32] D. D. Khalyavin, S. W. Lovesey, P. Maneul, F. Kruger, S. Rosenkranz, J. M. Allred, O. Chmaissem, and R. Osborn, Phys. Rev. B 90, 174511 (2014)

[33] E. Böhmer, F. Hardy, L. Wang, T. Wolf, P. Schweiss, C. Meingast, Nature Comm. 6, 7911 (2015).

[34] Xiaoyu Wang, Jian Kang, Rafael M. Fernandes, Phys. Rev. B 91, 024401 (2015).

[35] Maria N. Gastiasoro and Brian M. Andersen, Phys. Rev. B 92, 140506(R) (2015).

[36] Lihua Pan, Jian Li, Yuan-Yen Tai, Matthias J. Graf, Jian-Xin Zhu, and C. S. Ting, Phys. Rev. B 88, 214510 (2013).

[37] C. Castellani, C. R. Natoli, and J. Ranninger, Phys. Rev. B 18, 4945 (1978).

[38] Y. Y. Tai, J.-X. Zhu, J. G. Matthias, and C. S. Ting, Europhys. Lett. 103, 67001 (2013).

[39] P. Ghaemi, F. Wang, and A. Vishwanath, Phys. Rev. Lett. 102, 157002 (2009).

[40] X. Zhang, Y. S. Oh, Y. Liu, L. Yan, K. H. Kim, R. L. Greene, and I. Takeuchi, Phys. Rev. Lett. 102, 147002 (2009).

[41] K. Seo, B. A. Bernevig, and J. Hu, Phys. Rev. Lett. 101, 206404 (2008).

[42] Lihua Pan, Jian Li, Yuan-Yen Tai, Matthias J. Graf, Jian-Xin Zhu, and C. S. Ting, Phys. Rev. B 90, 134501 (2014).

[43] Kazuhiro Fujita, Mohammad H. Hamidian, Stephen D. Edkins, Chung Koo Kim, Yuhki Kohsaka, Masaki Azuma, Mikio Takano, Hidenori Takagi, Hiroshi Eisaki, Shin-ichi Uchida, Andrea Allais, Michael J. Lawler, Eun-Ah Kim, Subir Sachdev, and J. C. Séamus Davis, PNAS 111,E3026 (2014)

[44] M. H. Hamidian, S. D. Edkins, Chung Koo Kim, J. C. Davis, A. P. Mackenzie, H. Eisaki, S. Uchida, M. J. Lawler, E.-A. Kim, S. Sachdev & K. Fujita, Nat. Phys. 12, 150 (2016).

[45] Jiun-Haw Chu, James G. Analytis, Chris Kucharczyk, and Ian R. Fisher, Phys. Rev. B 79, 014506 (2009).